Materials Advances

ROYAL SOCIETY OF CHEMISTRY

COMMUNICATION

View Article Online
View Journal | View Issue

Check for updates

Cite this: *Mater. Adv.*, 2022, 3, 7508

Received 20th July 2022,
Accepted 12th September 2022

DOI: 10.1039/d2ma00837h

rsc.li/materials-advances

Deformable bi-compartmental particles and their application in controlling electric conductivity†

Qiang Zhang,‡[a] Yafei Yang,‡[a] Huijuan Yan[b] and Jiguang Liu*[a]

Deformable PNIPAM/PTMPTA and PEDOT@PNIPAM/Fe_3O_4@PTMPTA bi-compartmental particles were fabricated continuously in a microfluidic device, which exhibit deformed shapes due to the swelling of PNIPAM. The tunable ratio of the two compartments manipulates the particles' electric resistance. The PEDOT@PNIPAM/Fe_3O_4@PTMPTA functional particles undergo a synchronized rotation under a magnetic field, which further modulates their electrical conductivity.

Bi-compartmental particles consisting of two different compartments have attracted much attention due to their unique anisotropic and directional features by integrating different properties into one micro-particle. Not only can the two different compartments provide different surface properties,[1,2] they can also make the particle change shape,[3] directionality[4] or tropism,[5] which result in many new functions in biomedical areas,[6–9] micromotors,[10,11] or reflective cooling.[12]

Recently, some eye-catching properties have appeared in bi-compartmental particles responsive to electric fields. On top of their self-assembly behaviour under electric fields,[13,14] they could move under electric fields,[15] albeit usually with low conductivity; this leads to new functions, such as photochemically powered micromotors,[15] charge electrophoresis,[16] and rotation of particles.[17] Such change of electric conductivity of particles has wide applications in wearable sensors or biosensors, as well.[18]

At the same time, bi-compartmental particles responsive to magnetic fields also exhibit a fascinating character of synchronized rotation[19] and synchronized self-assembly behavior,[20] leading to many functions and applications, such as magnetically induced thermophoresis,[19] reconfigurable materials,[21,22] and e-ink displays.[23–25] Based on motion, bi-compartmental particles recently demonstrated "magic" properties in surface walking,[26] building molecular-analogue photonic crystal structures,[27] and the change of photonic properties.[28] The asymmetric magnetic property of one of the compartments that drives the rotation of particles has potential functions in changing the behaviour of another compartment, potentially resulting in new sensing properties.

Microfluidic technology has many advantages in preparing bi-compartmental particles, *e.g.*, in controlling particle size or composition, by which many particles have been prepared, such as polystyrene-Fe_3O_4/poly(vinylacetate),[29] polydiacetylene-1,2-dipalmitoyl-*sn-glycero*-3-galloyl/magnetic particles in different alginates,[30] and silica particles in ethoxylated trimethylolpropane triacrylate (ETPTA)/barium ferrite nanoparticles in a silicone precursor,[31] or in another ETPTA.[32] We hypothesize that the combination between conductivity and magnetic performance could further add to their functions and bring about wide applications.

We previously reported that functional substances, *e.g.*, conductive polyaniline and photochromic tungsten oxide, could be embedded into *N*-isopropylacrylamide (NIPAM)-based polymers due to the swelling ability of poly(*N*-isopropylacrylamide) (PNIPAM).[33–35] Moreover, the swelling PNIPAM could provide flexibility and temperature responsiveness, too. Here, bi-compartmental particles with electric conductivity and magnetic performance were fabricated by integrating functional substances into NIPAM-based polymers in a microfluidic device, which exhibits a smart electric conductivity under external magnetic fields.

As shown in Fig. 1 and Fig. S1 (ESI†), the home-made microfluidic device consists of a single silicon chamber and two drilled inlets for introducing solutions by syringe pumps. An aqueous solution with 10 wt% NIPAM, 1 wt% *N,N'*-methylenebisacrylamide (BIS) and 5 wt% 2-hydroxy-1-(4-(2-hydroxyethoxy)phenyl)-2-methylpropane-1-one (HEMO) was prepared, named as NIPAM solution. Meanwhile, trimethylolpropane triacrylate (TMPTA) containing 5 wt% 2-hydroxy-2-methylpropiophenone

[a] *School of Materials Design and Engineering, Beijing Institute of Fashion Technology, No. 2 Yinghua Road, Chaoyang District, Beijing, 100029, P. R. China. E-mail: J.Liu@bift.edu.cn*
[b] *CAS key Laboratory of Molecular Nanostructure and Nanotechnology, Institute of Chemistry, Chinese Academy of Sciences, No. 2 Zhongguancun North 1st Street, Beijing, 100190, P. R. China*

† Electronic supplementary information (ESI) available. See DOI: https://doi.org/10.1039/d2ma00837h

‡ Equal contribution.

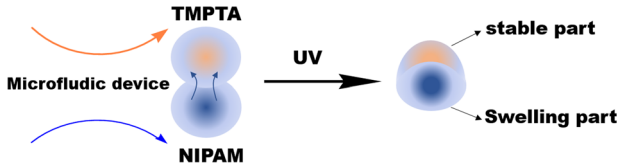

Fig. 1 A schematic illustrating the preparation of deformable bi-compartmental polymer particles or hybrid particles based on PNIPAM/PTMPTA.

(HMPO) was used as the TMPTA solution. The NIPAM solution and TMPTA solution were respectively used as the two dispersed phases. Dimethyl silicone was used as a continuous phase. As per the scheme in Fig. 1, the crosslinking poly(*N*-isopropylacrylamide), *i.e.*, PNIPAM, polymer will be produced by the copolymerization of NIPAM and BIS initiated by HEMO under UV light; meanwhile poly(trimethylolpropane triacrylate), *i.e.*, PTMPTA, will be produced *via* the self-crosslinked polymerization of TMPTA initiated by HMPO under UV light. Bi-compartmental polymer particles can be produced continuously (Video S1, ESI†) by the combination between PNIPAM and PTMPTA due to monomer diffusion.

Bi-compartmental particles with a diameter of around 300 μm were produced when the flow rates of the NIPAM solution, TMPTA solution and continuous phase were 0.1 mL h^{-1}, that is, the flow ratio of NIAPM solution to TMPTA solution (N/T ratio) was 1 : 1. In a polarized microscopic image, every particle consists of a dark part and a bright white part (Fig. 2a), with similar sizes. A series of bi-compartmental polymer particles with different sizes were prepared with a fixed N/T ratio at 1 : 1 by changing the flow rate of the continuous phase (Fig. S2, ESI†). The two compartments in all samples have a similar size; however, the total size of the bi-compartmental particles gradually reduced from 300 μm to 100 μm when the flow rate of the continuous phase increased from 0.1 mL h^{-1} to 0.25 mL h^{-1}.

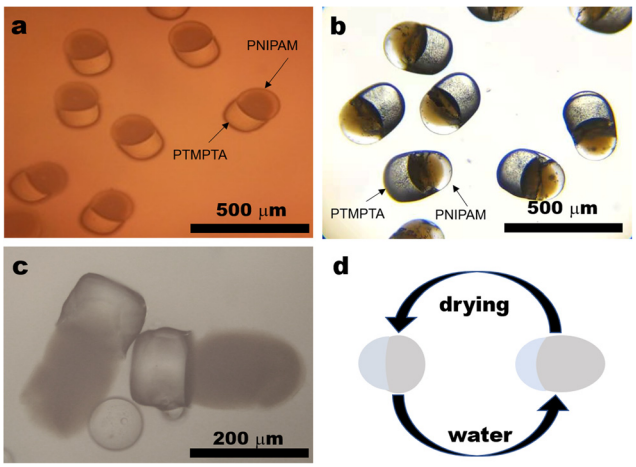

Fig. 2 PNIPAM/PTMPTA bi-compartmental polymer particles. (a) The polarized microscopic image of bi-compartmental polymer particles in dimethyl silicon; (b) the reflection microscopic image of bi-compartmental polymer particles; (c) the swollen particles in water; (d) the schematic deformation of the bi-compartmental particles. The flow rate of the silicon continuous phase was kept as 0.1 mL h^{-1} and the N/T ratio was 1 : 1.

The volume ratio of the two compartments in the bi-compartmental particles could be tuned by changing the N/T ratio with a fixed flow rate of continuous phase. When the N/T ratio was at 1 : 4, the colorless, hard part takes the dominant position (Fig. S3a, ESI†). The dark part gradually enlarges (Fig. S3b–d, ESI†) with increasing N/T ratios. The black part becomes dominant in the bi-compartmental particles when the N/T ratio is 1.1 : 0.9 or 1.2 : 0.8 (Fig. S3c and d, ESI†). This result confirms that the black part is PNIPAM from NIPAM solution while the bright part is PTMPTA from TMPTA solution.

The black compartment in polarized microscopy looks transparent in reflection mode while the bright part in polarized mode displays a brighter metallic colour in reflection mode (Fig. 2b). If a picture of particles is taken in a transmitted light mode, the black compartment in polarized microscopy becomes a soft white part while the bright part in polarized mode becomes a transparent hard part (Fig. S4, ESI†). If the particles were put into water, the dark transparent part in reflection mode swells significantly (Fig. 2c), which is a typical character of PNIPAM while the stable part with a brighter metallic colour in reflection mode could be attributed to PTMPTA. The shape change can be illustrated in Fig. 2d.

If 5 wt% magnetic nanoparticles were dispersed into TMPTA solution while the NIPAM solution was the same as the above, the hard PTMPTA part of the bi-compartmental particles became orange (Fig. S5, ESI†), indicating that magnetic nanoparticles mainly dispersed into the PTMPTA part. A minor amount of magnetic particles could diffuse into the PNIPAM part, as shown in the image of Fig. S5 (ESI†). These magnetic PNIPAM/Fe_3O_4@PTMPTA bi-compartmental particles could rotate under a magnetic field (Video S2, ESI†).

Furthermore, 3,4-ethylenedioxythiophene (EDOT) and polystyrene sulfonic acid were introduced into the above NIPAM solution for a NIPAM-EDOT solution (*i.e.*, NE solution), while magnetic TMPTA solution (*i.e.*, MT solution) was prepared with 5 wt% magnetic Fe_3O_4 particles and TMPTA solution. With the flow ratio of NE solution to MT solution at 1 : 1, *i.e.*, NE ratio at 50%, PEDOT@PNIPAM/Fe_3O_4@PTMPTA bi-compartmental hybrid particles were fabricated under UV irradiation since EDOT could be polymerized into electrically conductive poly(3,4-ethylenedioxythiophene) (PEDOT) inside the PNIPAM part, while Fe_3O_4 will exists in the PTMPTA part. As shown in Fig. 3a, all such particles consisted of an orange compartment and a blue compartment. The blue part is attributed to the PEDOT@PNIPAM compartment, the colour of which is from PEDOT. The orange part could be attributed to the Fe_3O_4@PTMPTA compartment, the colour of which is from Fe_3O_4. A few Fe_3O_4 nanoparticles maybe appear on the PEDOT@PNIPAM part due to their diffusion (Fig. S6a, ESI†).

After drying, the shape of the PEDOT@PNIPAM/Fe_3O_4@PTMPTA bi-compartmental particles morphs as the blue PEDOT@PNIPAM compartment collapses (Fig. S6b, ESI†), but the part of Fe_3O_4@PTMPTA stays intact. The dried PEDOT@PNIPAM part appears less than the Fe_3O_4@PTMPTA part since the content of

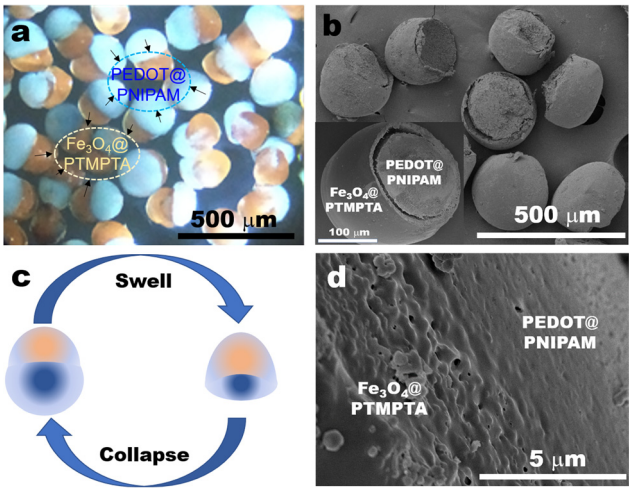

Fig. 3 PNIPAM@PEDOT/Fe_3O_4@PTMPTA bi-compartmental particles with NE ratio at 50%. (a) Microscopic image of the bi-compartmental particles in ethanol; (b) SEM image of the dried bi-compartmental particles; (c) schematic illustration of the deformation of the bi-compartmental particles; (d) the interface between two compartments of a bi-compartmental particle. The flow rate of the continuous phase and that of the dispersed phases were kept at 0.2 mL h^{-1}.

monomers in NE solution is much less than 50%, although the volume of the wet PEDOT@PNIPAM seems larger in solvent. As shown in the SEM image of Fig. 3b, the shape of Fe_3O_4@PTMPTA remains a stable hemispheric shape, similar to that in Fig. 3a. Meanwhile, the PEDOT@PNIPAM part in the dried particles almost disappears from shrinkage (Fig. 3b) so that only a little small bulge remains. The shape change is summarized in schematic Fig. 3c. The surface of the Fe_3O_4@PTMPTA part is smooth, but the interface between the Fe_3O_4@PTMPTA part and the PEDOT@PNIPAM part may become coarse (Fig. 3d), which could be attributed to the existence of Fe_3O_4.

Keeping the flow rate of the continuous phase and the total flow rate of the dispersed phases respectively at 0.2 mL h^{-1}, a series of functional bi-compartmental particles were prepared with different NE ratios. The PEDOT@PNIPAM ratio in the bi-compartmental particles increases with increasing NE ratios (Fig. S7a–c, ESI†), with an accompanying decrease in Fe_3O_4@PTMPTA size. That is, the volume ratio of the two compartments can be tuned by controlling the relative flow rates of the two solutions. However, the PEDOT@PNIPAM part in the dried sample was smaller than the Fe_3O_4@PTMPTA part even if the NE ratio was more than 50%, as shown in the SEM images (Fig. S8, ESI†). We note that the whole volume of the wet PEDOT@PNIPAM/Fe_3O_4@PTMPTA bi-compartmental particles increased slightly with increasing NE ratios (Fig. S7, ESI†), which was attributed to the swollen PNIPAM component.

The compositions of the particles were characterized with thermogravimetric analysis (TGA). As a comparison, the pristine PTMPTA, PEDOT and PNIPAM polymers were also analysed (Fig. S9a, ESI†). PNIPAM degraded from 350 °C to *ca.* 420 °C, with a residue of *ca.* 4.9 wt%. PTMPTA decomposed from *ca.* 400 °C to 450 °C, which had a residue of *ca.* 14.4 wt%. PEDOT had a very high residue (*ca.* 32.5 wt%) and a continuous thermolysis after 250 °C. In the TGA curve of PEDOT@PNIPAM/Fe_3O_4@PTMPTA bi-compartmental particles with an NE ratio at 50%, there are three decomposition steps after 210 °C (Fig. S9b, ESI†), indicating at least three different polymer compositions. In addition, the weight loss before 210 °C could be ascribed to water and a little unreacted monomer. The two weight losses at *ca.* 300–420 °C should be caused by the decomposition of PEDOT and PNIPAM, which is around 30 wt%. The third weight loss (*ca.* 50 wt%) at *ca.* 420–460 °C was attributed to the decomposition of PTMPTA. All decomposition temperatures became higher than those of the pristine polymers, which may be attributed to the effective radical quenching.[36] More than 10 wt% residue was mainly attributed to Fe_3O_4. The existence of Fe_3O_4 could be proved in Fig. S10 (ESI†), in which, these particles could be attracted onto a side wall when a magnet was placed there.

The compositions of the PEDOT@PNIPAM/Fe_3O_4@PTMPTA bi-compartmental particles were further analysed with Elemental Analysis by Combustion (EAC), the results of which are summarized in Table S1, ESI.† Nitrogen and sulphur came from PNIPAM and PEDOT, respectively, the amount of which increases with increasing NE ratio (Fig. S11a and b, ESI†). The ratio of nitrogen to carbon (N/C) and the ratio of sulphur to carbon (S/C) were calculated, which synchronously increased with the increasing NE ratio (Fig. S11c, ESI†). This result is consistent with the increasing ratio of the PEDOT@PNIPAM compartment in Fig. S7 (ESI†).

Since PEDOT is a conductive polymer, the electric resistance of PEDOT@PNIPAM/Fe_3O_4@PTMPTA bi-compartmental particles could be measured in absolute ethanol. The resistance of absolute ethanol was higher than the measuring limit. One hundred bi-compartmental particles with an NE ratio of 50% in absolute ethanol were placed with a random array between two ITO glass slides as electrodes. The distance of two glass slides was adjusted to 300 μm by a lift table. After 2 minutes of calibration standing time, the electric resistance was read, which was *ca.* 38 MΩ (Fig. S12a, ESI†). For bi-compartmental particles with different NE ratios, the electric resistance almost decreased linearly to 17 MΩ as the NE ratio increased to 80%, *i.e.*, with increasing PEDOT@PNIPAM composition. If 500 particles were used, the measured resistance reduced from 5.3 MΩ to 3.7 MΩ with the NE ratio increasing from 50% to 80% (Fig. S12b, ESI†). The results assured the conductivity of the bi-compartmental hybrid particles, *i.e.*, the more particles, the lower the resistance, and the effect of PEDOT, *i.e.*, the more PEDOT, the better the conductivity.

The synchronized rotation of these particles driven by a magnetic field can be realized due to the presence of Fe_3O_4. As shown in Video S3 (ESI†), all bi-compartmental particles rotate in the same direction accompanying the changed direction of the magnet, indicating a response to a magnetic field. The rotation of bi-compartmental particles provides the possibility of resistance variation by controlling the orientation of the conductive PEDOT@PNIPAM part (Fig. 4a).

It was experimentally found that the resistance of 100 bi-compartmental particles with a random array gradually

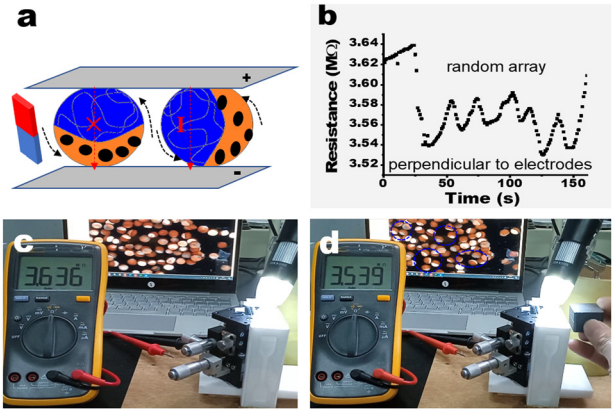

Fig. 4 The conductivity of PEDOT@PNIPAM/Fe_3O_4@PTMPTA bi-compartmental particles. (a) Schematic illustration of controlling the electric resistance by a magnet; (b) the oscillating resistance of the bi-compartmental particles driven by a magnetic field; (c) the resistance of the bi-compartmental particles without a magnet; (d) the resistance of the bi-compartmental particles perpendicular to electrodes under a magnetic field.

increased from 3.546 MΩ to 3.639 MΩ in 80 seconds without any magnetic field (Fig. S13 and Video S4, ESI†), which may be attributed to the ohmic heating. When a magnet parallel to the glass slides was applied, these particles rotated in a synchronized mode (Video S4, ESI†). When the PEDOT@PNIPAM part of the more bi-compartmental particles connected to the two conductive glass slides, the resistance immediately decreased from 3.639 MΩ to 3.539 MΩ with the rotation of particles (Fig. 4b and Video S4, ESI†). After a while, the resistance again started to increase due to ohmic heating. The resistance, however, can be recurrently reduced as the magnet is placed to and removed from the glass slides. The screen snapshots are shown in Fig. 4c and d, respectively, indicating different resistances before and after the rotation of these particles. Compared with Fig. 4c, there were more particles perpendicular to the glass slides in Fig. 4d, while the measured resistance is relatively lower. The oscillating resistance accompanying the rotation of the bi-compartmental particles is summarized in Fig. 4b, indicating an electric resistance responsive to a magnetic field. We note that if these particles were dried due to the evaporation of the solvent or under heating, the current would be interrupted due to the collapse of the PEDOT@PNIPAM compartment, as shown in Fig. S14 (ESI†). This could potentially be useful in detecting moisture.

In summary, bi-compartmental PNIPAM/PTMPTA polymer particles and PEDOT@PNIPAM/Fe_3O_4@PTMPTA hybrid functional particles were continuously fabricated in a microfluidic device, in which the PNIPAM or PEDOT@PNIPAM compartments could swell or collapse. The PEDOT@PNIPAM/Fe_3O_4@PTMPTA bi-compartmental particles exhibited conductivity dependent on the NE ratio and orientation. These particles could rotate under a magnetic field, resulting in an oscillation of their electrical conductivity. These bi-compartmental particles responsive to an electric field and a magnetic field will have wide potential applications in constructing functional materials, fabricating sensors, and biological imaging.

Author contributions

Q. Zhang: investigation, data curation, writing – original draft; Y. Yang: investigation, data curation, validation; H. Yan: investigation, resources of characterization; J. Liu: conceptualization, writing–review & editing and supervision.

Conflicts of interest

There are no conflicts to declare.

Acknowledgements

We thank the Key Program Jointly Supported by Beijing Municipal Commission of Education and Municipal Natural Science Foundation (No. KZ202010012020).

Notes and references

1 A. Kirillova, C. Marschelke, J. Friedrichs, C. Werner and A. Synytska, *ACS Appl. Mater. Interfaces*, 2016, **8**, 32591–32603.
2 B. D. Frank, M. Perovic, S. Djalali, M. Antonietti, M. Oschatz and L. Zeininger, *ACS Appl. Mater. Interfaces*, 2021, **13**, 32510–32519.
3 J. Liu and J. Huskens, *Chem. Commun.*, 2015, **51**, 2694–2697.
4 Y. Yi, L. Sanchez, Y. Sanchez and Y. Yu, *Analyst*, 2016, **141**, 3526–3539.
5 P. Serra and P. Santamaria, *Clin. Immunol.*, 2015, **160**, 3–13.
6 I. Mirza and S. Saha, *ACS Appl. Bio Mater.*, 2020, **3**, 8241–8270.
7 E. E. Ekanem, S. A. Nabavi, G. T. Vladisavljević and S. Gu, *ACS Appl. Mater. Interfaces*, 2015, **7**, 23132–23143.
8 X. Li, M. L. Zhou, Y. Wei, A. M. El-Toni, F. Zhang and D. Y. Zhao, *J. Am. Chem. Soc.*, 2014, **136**, 15086–15092.
9 A. C. Misra, S. Bhaskar, N. Clay and J. Lahann, *Adv. Mater.*, 2012, **24**, 3850–3856.
10 S. Park and G. Yossifon, *ACS Sens.*, 2020, **5**, 936–942.
11 X. Ma, S. Jang, M. N. Popescu, W. E. Uspal, A. Miguel-López, K. Hahn, D. P. Kim and S. Sánchez, *ACS Nano*, 2016, **10**, 8751–8759.
12 Z. J. Zhu, J. D. Liu, C. Liu, X. J. Wu, Q. Li, S. Chen, X. Zhao and A. D. Weitz, *Small*, 2020, **16**, 1903939.
13 S. Gangwal, O. J. Cayre and O. D. Velev, *Langmuir*, 2008, **24**, 13312–13320.
14 S. Gangwal, A. Pawar, I. Kretzschmar and O. D. Velev, *Soft Matter*, 2010, **6**, 1413–1418.
15 C. Zhou, H. P. Zhang, J. Y. Tang and W. Wang, *Langmuir*, 2018, **34**, 3289–3295.
16 K. J. M. Bishop, A. M. Drews, C. A. Cartier, S. Pandey and Y. Dou, *Langmuir*, 2018, **34**, 6315–6327.
17 X. Li, Y. T. Yang, L. J. Wu, Y. C. Li, M. Y. Ye, Z. Q. Chang, D. Q. Meng and C. A. Serra, *Mater. Lett.*, 2015, **142**, 258–261.
18 J. R. Camargo, L. O. Orzari, D. A. G. Araújo, P. R. de Oliveira, C. Kalinke, D. P. Rocha, A. Luiz dos Santos, R. M. Takeuchi,

R. A. A. Munoz, J. A. Bonacin and B. C. Janegitz, *Microchem. J.*, 2021, **164**, 105998.
19 L. Baraban, R. Streubel, D. Makarov, L. Han, D. Karnaushenko, O. G. Schmidt and G. Cuniberti, *ACS Nano*, 2013, **7**, 1360–1367.
20 J. Yan, M. Bloom, S. C. Bae, E. Luijten and S. Granick, *Nature*, 2012, **491**, 578–581.
21 C. Q. Yu, J. Zhang and S. Granick, *Angew. Chem., Int. Ed.*, 2014, **126**, 4453–4456.
22 F. Soyka, O. Zvyagolskaya, C. Hertlein, L. Helden and C. Bechinger, *Phys. Rev. Lett.*, 2008, **101**, 208301.
23 Q. Chen, E. Diesel, J. K. Whitmer, S. C. Bae, E. Luijten and S. Granick, *J. Am. Chem. Soc.*, 2011, **133**, 7725–7727.
24 B. A. Grzybowski, H. A. Stone and G. M. Whitesides, *Nature*, 2000, **405**, 1033–1036.
25 C. Q. Yu, J. Zhang and S. Granick, *Angew. Chem., Int. Ed.*, 2014, **53**, 4364–4367.
26 T. Li, A. Zhang, G. Shao, M. Wei, B. Guo, G. Zhang, L. Li and W. Wang, *Adv. Funct. Mater.*, 2018, **28**, 1706066.
27 S. N. Yin, S. Yang, C. F. Wang and S. Chen, *J. Am. Chem. Soc.*, 2016, **138**, 566–573.
28 S. K. Nam, J. B. Kim, S. H. Han and S. H. Kim, *ACS Nano*, 2020, **14**, 15714–15722.
29 R. A. Nuumani, S. K. Smoukov, G. Bolognesi and G. T. Vladisavljević, *Langmuir*, 2020, **36**, 12702–12711.
30 D. H. Kang, H. S. Jung, N. Ahn, S. M. Yang, S. Seo, K. Y. Suh, P. S. Chang, N. L. Jeon, J. Kim and K. Kim, *ACS Appl. Mater. Interfaces*, 2014, **6**, 10631–10637.
31 S. K. Nam, J. B. Kim, S. H. Han and S. H. Kim, *ACS Nano*, 2020, **14**, 15714–15722.
32 Y. J. Zhao, H. C. Gu, Z. Y. Xie, H. C. Shum, B. P. Wang and Z. Z. Gu, *J. Am. Chem. Soc.*, 2013, **135**, 54–57.
33 J. Liu, J. Liu, F. Ma and J. Liu, *ACS Appl. Polym. Mater.*, 2019, **1**, 152–159.
34 J. Liu, Q. Zhang and J. Liu, *Acta Polym. Sin.*, 2019, **50**, 695–701.
35 Q. Zhang, R. Wang, Y. Lu, Y. Wu, J. Yuan and J. Liu, *ACS Appl. Mater. Interfaces*, 2021, **13**, 4220–4229.
36 T. Uemura, T. Kaseda, Y. Sasaki, M. Inukai, T. Toriyama, A. Takahara, H. Jinnai and S. Kitagawa, *Nat. Commun.*, 2015, **6**, 7473.